Segmentation of Head and Neck Lymph Node Regions for Radiotherapy Planning Using Active Contour-Based Atlas Registration

Subrahmanyam Gorthi, Valérie Duay, Nawal Houhou, Meritxell Bach Cuadra, Ulrike Schick, Minerva Becker, Abdelkarim S. Allal, and Jean-Philippe Thiran, *Senior Member, IEEE*

***Abstract*—In this paper, we present the segmentation of the head and neck lymph node regions using a new active contour-based atlas registration model. We propose to segment the lymph node regions without directly including them in the atlas registration process; instead, they are segmented using the dense deformation field computed from the registration of the atlas structures with distinct boundaries. This approach results in robust and accurate segmentation of the lymph node regions even in the presence of significant anatomical variations between the atlas-image and the patient's image to be segmented. We also present a quantitative evaluation of lymph node regions segmentation using various statistical as well as geometrical metrics: sensitivity, specificity, dice similarity coefficient and Hausdorff distance. A comparison of the proposed method with two other state of the art methods is presented. The robustness of the proposed method to the atlas selection, in segmenting the lymph node regions, is also evaluated.**

***Index Terms*—Atlas-based segmentation, head and neck, IMRT, lymph node regions, non-rigid registration, radiotherapy.**

I. Introduction

INTENSITY-modulated radiotherapy (IMRT) is the ultimate high precision technique to accurately deliver X-ray radiation treatment for different tumor locations of the patients. However, one of the significant obstacles in the widespread implementation of IMRT, for head and neck (H&N) cancer, concerns the complexity of target definition. In the case of H&N carcinomas radiotherapy, besides the gross tumor volume, the radiation oncologist has to segment the clinical target volume and the complicated planning target volume which contains different lymph node levels. Each lymph node level or group of levels correspond to a potential area of spread for a given tumor sublocation. Since the IMRT approach prerequisites the segmentation of all the volumes to be treated as well as the organs at risk, it is easy to understand that its routine use for H&N tumors is not common at the present time. Besides the precise contouring of primary H&N tumors that is often difficult, the accurate, reproducible and time-efficient contouring of elective nodal risk regions represents an even greater challenge. The tentative to implement lymph nodes levels segmentation in the clinical environment were initially based on the translation of the surgical lymph nodes levels to CT-based regions which meant meticulous segmentation of each CT regions on each slice of the planning CT scan, a laborious process that was considered as incompatible with a routine clinical practice [1]. Indeed, experienced H&N cancer specialists generally spend several hours to fully contour and refine desired targets for a single H&N IMRT case. In a study reported by Song *et al.* [2], the average physician working time to design a H&N treatment contours for the target definition was 2.7 h for IMRT approach compared to 0.3 h for the conventional three field plan. In summary, the major challenge in the routine clinical implementation of IMRT for H&N region is to delineate the lymph nodes automatically and accurately.

Grégoire *et al.* [3] presented guidelines for delineating the lymph nodes in the H&N region. Fig. 4 shows the manually delineated lymph node levels: IA, IB-left, IB-right, IIA-left, IIA-right, IIB-left, IIB-right, III-left, III-right, IV-left, IV-right, VA-left, VA-right, VB-left, VB-right, and VI in the computed tomography (CT) images. 3-D volumes of these lymph nodes are shown in Fig. 8. Most of these lymph nodes do not have distinct boundaries; rather they are defined with respect to other distinct landmark structures in the H&N region and hence posing challenges in the automated segmentation.

The lymph node segmentation techniques that have been reported so far can be broadly classified into two categories. The first category of techniques assume that at least a portion of the lymph node to be segmented has a distinct boundary with the surrounding structures. The second category of techniques do not assume the existence of any such distinct boundaries.

In the first category, Rogowska *et al.* [4] used various basic techniques like threshold selection, sobel/watershed technique and deformable contour algorithm for the segmentation of lymph nodes. Their evaluation was on synthetic images. In [5], Honea *et al.* semi-automatically segmented the lymph nodes with slice-wise active contours and active surface models. Their evaluation was also on synthetic images. In [6], Yan *et al.* proposed an

Manuscript received April 15, 2008; revised October 15, 2008. Current version published February 19, 2009. This work was supported in part by the Swiss National Research Funds under Grant 3252B0-107873 and by the Center for Biomedical Imaging (CIBM) of the Geneva-Lausanne Universities and the EPFL, as well as the foundations Leenaards and Louis-Jeantet. The associate editor coordinating the review of this manuscript and approving it for publication was Dr. Jianhua Yao.

S. Gorthi, N. Houhou, M. Bach Cuadra, and J.-P. Thiran are with the Signal Processing Laboratory (LTS5), Ecole Polytechnique Fédérale de Lausanne (EPFL), Lausanne, Switzerland (e-mail: subrahmanyam.gorthi@epfl.ch; nawal.houhou@epfl.ch; meritxell.bach@epfl.ch; jp.thiran@epfl.ch).

V. Duay is with the Institute of Bio-Engineering, University of Applied Sciences Western Switzerland (HES-SO Genéve), Geneva, Switzerland (e-mail: valerie.duay@hesge.ch).

U. Schick, M. Becker, and A. S. Allal are with the Department of Radiation Oncology, University Hospital Geneva, Switzerland (e-mail: Ulrike.Schick@hcuge.ch; Minerva.Becker@hcuge.ch; Abdelkarim.Allal@hcuge.ch).

Color versions of one or more of the figures in this paper are available online at http://ieeexplore.ieee.org.

Digital Object Identifier 10.1109/JSTSP.2008.2011104

improved 2-D fast marching method with an intensity weighted speed term. [7] extended it to 3-D images using a similar idea with watershed transform. In both [6], [7], boundary leaking is avoided through a hard stopping criterion, by manually bounding a circle around the lymph node; the circle should be very close to the actual boundary of the lymph node. In [8], Dornheim *et al.* proposed a mass-spring model for 3-D lymph node segmentation, and the formulation is based on the characteristic gray value range, directed contour information and shape knowledge.

The second category of techniques are atlas-based segmentation methods. Atlas-based methods have become a standard paradigm in medical image segmentation for exploiting prior anatomical knowledge. The atlas is a reference image in which structures of interest, here the lymph nodes, have been carefully segmented, usually by hand. To segment a new image, a dense deformation field that registers (i.e., puts in point-to-point correspondence) the atlas to the patient image is first computed. This transformation is then used to project labels assigned to the different structures from the atlas onto the patient image to be segmented. Thus, the segmentation problem is reduced to a registration problem. The registration task typically consists of first capturing the difference in positions between the atlas and the patient image. This is often done with an affine registration. Then, a non-rigid registration is used to compensate the normal anatomical variability between both the images. One of the main advantages of atlas-based methods compared to the segmentation techniques presented in the first category, is that the dense deformation field, interpolated on the whole image from the registration of visible image features, allows to easily estimate in the patient image, the position of structures with fuzzy or not visible contours. Atlas-based segmentation methods are thus particularly well suited for the lymph node regions segmentation.

The majority of atlas-based methods that have been proposed so far are developed for brain segmentation. Unfortunately, these methods are of limited use for lymph nodes segmentation due to the presence of high anatomical variability, particularly in the nodal regions. To cope up with this problem, Teng *et al.* [9] propose to use the BSpline algorithm of Mattes *et al.* [10] along with the landmark points. The landmark points are selected on the mandible and hyoid bones, because of their proximity to the lymph nodes, high contrast and consistency among the patients. These landmarks are used to initialize the deformation field at the start of every resolution level of the BSpline algorithm. The authors show that local constraints on the atlas registration lead to a more accurate delineation of the lymph nodes. The main drawback of this method is that it requires a pre-processing step including the segmentation of the bones of interest in the patient image, the extraction of the landmark points on the bones surfaces and the computation of landmarks correspondence between the atlas and the patient image. In [11], Commowick *et al.* try to better catch the high variability of the H&N region by using a mean atlas built from a database of 45 patients. The atlas is then registered to the patient image by using a block matching algorithm [12], [13]. However, this method shows limitations when the patient anatomy is too different from the mean atlas or when the structures of the patient image are drastically deformed by a lesion.

The model that we propose here to segment the lymph node regions, aims to combine the advantages of the dense deformation field computed by the non-rigid registration algorithms with local segmentation constraints derived from the active contour (AC) segmentation framework. Unlike many of the previous approaches, *the lymph nodes are not directly segmented* in this paper. Rather, *the lymph node regions are indirectly segmented* using the dense deformation field. The dense deformation field computed from the registration of visible image contours allows to easily estimate the position of structures with not well or without visible contours in the image such as the lymph node regions. On the other hand, the AC segmentation model is often able to delineate visible boundaries in a more accurate way than the segmentation method based on atlas registration. This is due to its global and local matching criteria that can exploit the image information directly linked to the objects to be extracted. The main advantage of our active contour-based registration model is that it can jointly perform the segmentation task and a registration task. Moreover, it allows to select structures to drive the registration process. These structures are chosen to be *consistent* between the atlas and the patient's image and *relevant* to find the position of the lymph node regions. Then, thanks to the AC framework, our algorithm allows to easily introduce prior knowledge, such as the intensity distribution or the admissible shapes on the objects selected to drive the atlas registration. Finally, we will show that our model is able to recover higher anatomical variability than the state of the art atlas registration methods that we have tested in this paper.

Quantification of automated segmentation results is an important aspect for comparing them with the existing results as well as for using them in practice. Statistical methods commonly used in medical image processing can often fail to detect errors in segmentation results. For instance, Popovic *et al.* [14] found that better values of sensitivity and specificity alone, which are commonly used metrics for evaluation, cannot always guarantee improvement in other important metrics like dice similarity coefficient and Hausdorff distance. Exhaustive quantitative evaluation of the H&N lymph node regions segmentation has not been reported so far. In this paper, we also present the quantitative evaluation of the results for each lymph node region, using various statistical and geometrical metrics. The evaluation is performed by comparing the automated segmentation results against the manually segmented lymph nodes by the radiation oncologist. The results from our active contour-based atlas registration model are also compared with two other state of the art methods.

The paper is organized as follows. In the next Section, we present our active contour-based registration model. In Section III, we describe our lymph node regions segmentation approach and also present the details of the dataset used for the evaluation. In Section IV, we present the qualitative and quantitative evaluation of the lymph node regions segmentation; the results are compared with the results from Demons registration model [15] and a radial basis function registration model [16]. The robustness of the proposed method to the atlas selection, in segmenting the lymph node regions is also evaluated. Finally, discussion and conclusions are presented in Section V.

II. METHOD

A. Our Active Contour-Based Atlas Registration Model

The main source of inspiration of our joint registration and segmentation algorithm is the partial derivative equation (PDE)-based method proposed by Vemuri *et al.* in [17] [1]. The formulation of their model is intuitively deduced from the general level set [2] evolution (1) introduced by Osher and Sethian in [19]

$$\frac{\partial \phi_d(x,t)}{\partial t} = \phi_{d,t}(x,t) = \nu(\phi_d(x,t))|\nabla \phi_d(x,t)| \qquad (1)$$

where ν is the velocity of the flow or speed function that contains the local segmentation and contour regularization constraints and ϕ_d is the signed distance function often used to represent implicitly the active contour (AC) by its zero level. The original idea brought by Vemuri's model is to replace, in (1), ϕ_d by the intensity function of the image to register (the moving image). Thus, the level sets considered in the segmentation process correspond to the contours naturally present in the moving image, i.e., the curves of high image gradient. A dense deformation field is then generated by tracking the deformation of these level sets during the segmentation process. The main advantage of this model using the intensity function, is to register any type of contours (closed, open, connected or disconnected) unlike the signed distance function that can only model closed and disconnected contours. However, this advantage can also be a drawback. Since all the level sets of the reference image are considered, inconsistencies between both images, e.g., local intensity differences between both images or a lesion in the patient image, can lead to misregistration. Moreover, since this contour representation does not permit to select consistent contours or closed regions in the atlas, Vemuri's model is limited to pixel-based segmentation forces only. That means that this model cannot use the typical segmentation forces of the AC framework such as boundary-based and region-based forces (see Section II-D) in the registration process.

Unlike [17], our registration model is able to use forces developed in the AC framework since it is based on the general level set approach [19]. Moreover, we propose to handle the registration of multiple regions by modeling the active contours with a label function.

B. Deformation Field Extraction

The general formulation of our model is derived from the tracking of the signed distance function motion with the optical flow (OF) approach [20]. The OF technique assumes that the brightness of the moving image, here the level set function ϕ_d, stays constant for small displacements and for a short period of time

$$\phi_d(x,t) = \phi_d(x+du, t+dt) \Rightarrow d\phi_d(x,t) = 0 \qquad (2)$$

where du is the instantaneous deformation vector field and $d\phi_d$ is the total derivative of ϕ_d. By using the chain rule, this optical flow constraint can be rewritten as the evolution equation of a vector flow

$$\frac{\partial u(x,t)}{\partial t} = -\frac{\phi_{d,t}}{|\bigtriangledown \phi_d|}\frac{\bigtriangledown \phi_d}{|\bigtriangledown \phi_d|} \qquad (3)$$

where $\phi_{d,t}$, given by (1), represents the variation of the level set function according to the desired forces such as supervised segmentation, shape prior knowledge or contour regularization. Thus, by introducing the evolution equation of the level set segmentation model (1) in (3), we obtain the following equation *merging the active contour segmentation framework with the image registration task*:

$$\frac{\partial u(x,t)}{\partial t} = -\nu(\phi_d(x,t))\frac{\bigtriangledown \phi_d}{|\bigtriangledown \phi_d|}. \qquad (4)$$

The level set function ϕ_d does not evolve with the usual finite difference scheme. Its position at time t is given by the deformation field $u(x,t)$ and the initial level set function $\phi_d(x,0)$ such that

$$\phi_d(x,t) := \phi_d(x+u(x,t),0) \qquad (5)$$

with $\phi_d(x,0)$ is the initial active contour position. This ensures that the evolution of the level set function exactly corresponds to the current deformation. Introducing (5) in (4) yields

$$\frac{\partial u(x,t)}{\partial t} = -\nu(\phi_d(x+u(x,t),0))\frac{\bigtriangledown \phi_d}{|\bigtriangledown \phi_d|}. \qquad (6)$$

This equation corresponds to *the general formulation of our AC-based atlas registration model*. It defines a displacement vector (or registration force) at each point of the level set function. The level set function models the contours of the objects selected in the atlas to drive its registration. We show in Sections II-C and II-D that a large variety of active contour segmentation models can be used in the registration process.

C. Label Function Representation

The signed distance function representation ϕ_d can be used with any type of forces derived from the active contour framework (see Section II.D). However, this representation can model only two regions. As we said, the intensity function representation proposed by Vemuri *et al.* in [17] can model any type of contours but it can only be used with pixel-based registration forces. To cope up with these limitations, we propose to represent the active contours selected in the atlas to drive its registration by a label function ϕ_L [3]. This label function permits to define an arbitrary number of regions as follows: $\phi_L : x \in \Omega_k \rightarrow \phi_L(x) = k, k \in [1,\ldots,n]$ if $x \in \Omega_k$, where Ω_k is the k^{th} labeled region and n is the number of regions. In this representation, active contours are modeled by the discontinuities of ϕ_L. The main advantage of the label function representation is to distinguish n regions by using only one function. However,

[1]There exists also a variational energy-based approach initiated by Yezzi *et al.* in [18] to combine registration to AC segmentation. We chose the PDE-based approach because it seems more flexible to solve joint registration and segmentation problems notably in the choice of the attractive and regularization terms composing the speed function.

[2]Level set method is a non-parametric model of the active contour technique.

[3]We note that in the active contours segmentation framework, the idea of using labels to perform a multi-phase segmentation has recently been presented (see for instance [21]). The difference with our work is that this representation has been proposed for particular variational energy-models and we present a scheme for any type of PDE-based models.

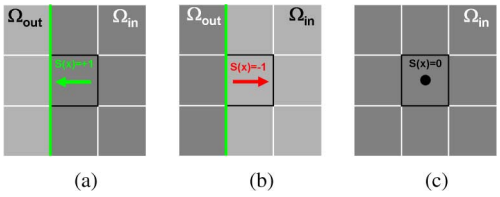

Fig. 1. Illustration of the function S. (a) $S(x) = 1$ Gradient is in the right direction. (b) $S(x) = -1$ Gradient direction has to be changed. (c) $S(x) = 0$ Gradient is null.

this representation does not contain the polarity information (information indicating the inside (Ω_{in}) and the outside (Ω_{out}) of a modeled region) necessary to compute the region-based forces of the AC segmentation framework. In order to generate the polarity information, we introduce a function "$S(x)$" in the general formulation of our model (6). The objective of this function is to adapt the orientation of the gradient $\bigtriangledown\phi_L$ based on local label values such that it always gives the polarity of the current region, i.e., $S(x) \bigtriangledown \phi_L$ is always oriented from the inside to the outside of the region. Fig. 1 illustrates the function $S(x)$. The green line enhances the interface between the light and dark regions. Each panel shows the current pixel (enhanced in bold) surrounding by its eight neighbors. The arrow shows the initial direction of the gradient. If neighbors have values larger or equal to $\phi_L(x)$, the gradient is already in the right direction and hence, $S(x) = +1$ [Fig. 1(a)]. If one neighbor has a value inferior to $\phi_L(x)$, the gradient direction is changed with $S(x) = -1$ [Fig. 1(b)]. Finally, if the neighborhood has the same value of $\phi_L(x)$, the gradient is null which means $S(x) = 0$ [Fig. 1(c)]. With the label function representation, the general formulation of our registration model (6) becomes

$$\frac{\partial u(x,t)}{\partial t} = -S(x)\nu(\phi_L(x+u(x,t),0))\frac{\bigtriangledown\phi_L}{|\bigtriangledown\phi_L|}. \quad (7)$$

The generalized evaluation (1) of the joint registration and segmentation model is proposed in [22]. It is used with a signed-distance-map representation in [23]. The main limitation of [22] and [23] is that they can model only two regions. The evaluation (1) is extended to multiple regions with the modified model (7), along with the label function representation. The preliminary discussions on this model with label function representation, and the initial results on 2-D images in registering structures with distinct boundaries, are presented in the conference paper [24]. The method used in this paper differs with [24] in the following aspects:

- [24] does not use any explicit regularization forces whereas in this paper, mean curvature forces (discussed later in this section) are used for regularization;
- [24] uses entropy-based region forces while mean-based region forces are used in this paper, as they are found to be more suitable for the segmentation of H&N region.

The main contribution of this paper is the application and evaluation of this method in the context of H&N lymph node regions segmentation. Please refer to [25] for a more detailed description of the generalized framework.

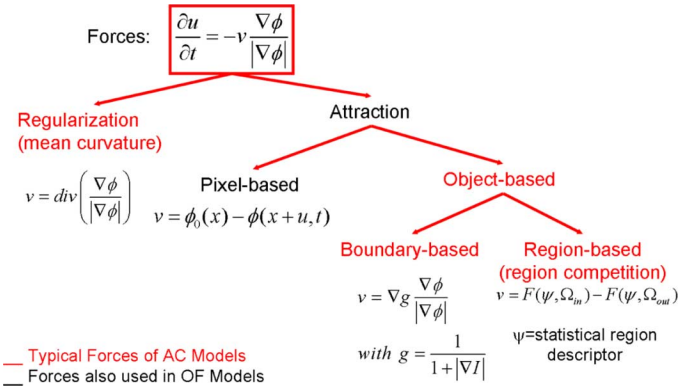

Fig. 2. Classification of the AC forces according to their effect in a contour matching process.

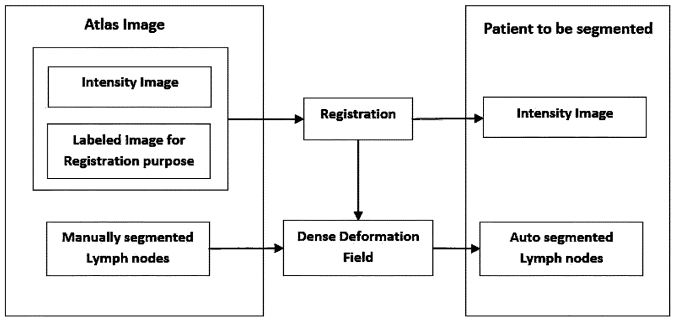

Fig. 3. Block diagram illustrating the proposed lymph node regions segmentation approach.

D. Registration/Segmentation Forces

Fig. 2 summarizes different types of forces coming from the AC segmentation framework that can still be used in the registration process. The most used *regularization force* of the AC framework is the mean curvature force. This force smoothens the level sets by minimizing their length. They can be applied on any type of contour representation. The *pixel-based forces* are based on the smallest image feature, the pixel value. They allow the local registration of the whole moving image domain or selected regions. Pixel-based forces are the typical segmentation forces of the OF model. In the AC model, these forces are rather used to include intensity or shape prior knowledge in a segmentation process. These forces can match any type of contours (closed or open) and can also be used with any type of representation. However, they are very sensitive to image noise and are limited to recover small deformations. *Object-based forces* can register image regions. If we apply an object-based force on each point of a signed distance function, every level set will collapse to the closest target contour in the target image. So, they need to be computed only on the zero level set of the signed distance function ϕ_d or around the interface of the labeled function ϕ_L. Finally, *region-based forces* are very efficient forces of the AC framework because they are less sensitive to noise than the *boundary-based forces*. They can also perform supervised segmentation, i.e., they can use prior knowledge extracted from a reference image. This region-based forces seems thus particularly well suited to register an atlas based on selected objects with visible boundaries. At each iteration of our algorithm, the

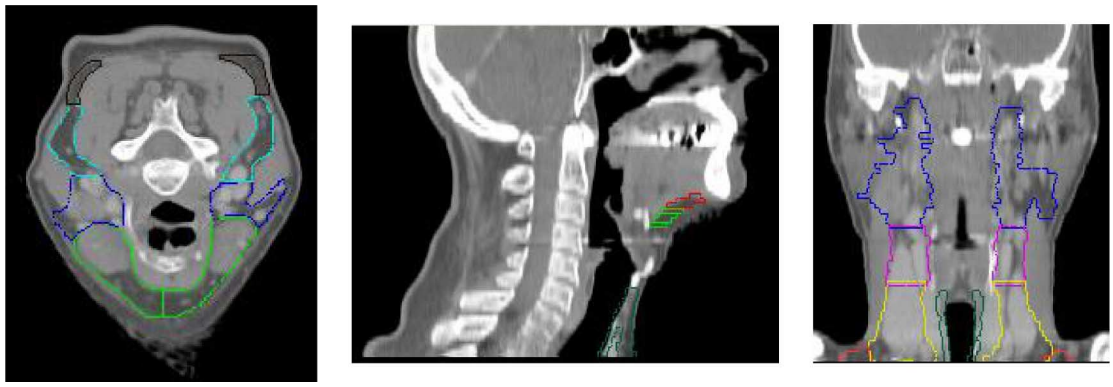

Fig. 4. Atlas image in the (I) Axial, (II) sagittal, and (III) coronal slices. Manually delineated lymph nodes are superposed over the atlas image.

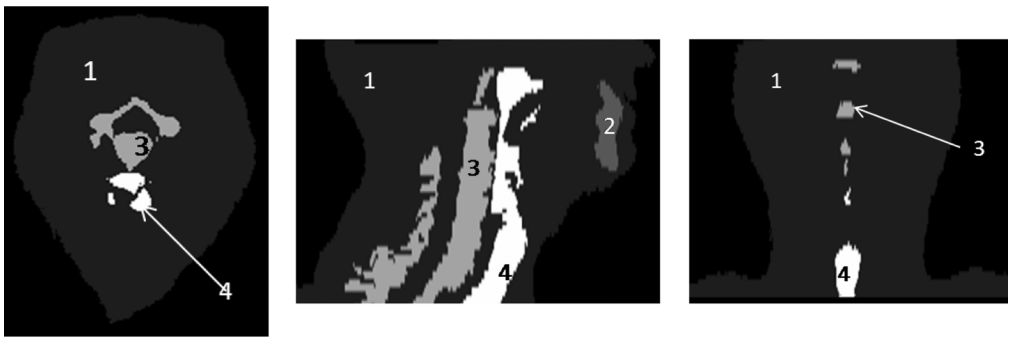

Fig. 5. Labeled image in the (I) Axial, (II) sagittal, and (III) coronal slices. The labeled structures in the image are (1) external-contour, (2) mandible, (3) vertebra, and (4) trachea.

displacement computed on the active contour is extended to the whole image by linear diffusion and thus influence the position of their surrounding objects. Finally, the registration process is speeded up by a multiresolution approach.

E. Atlas-Based Lymph Node Regions Segmentation Process

The whole lymph node regions segmentation process is illustrated in Fig. 3. Our active contour-based atlas algorithm is used to register the atlas to the patient images. First the structures of interest selected in the atlas to drive its registration are represented by a labeled function. This label function is shown in Fig. 5. It models the external contour of the image, mandible, vertebrae and trachea. These structures have been chosen for the following two reasons. First, they are closely located to the lymph nodes. Hence, their registration will influence the location of the lymph nodes. Then they have distinct boundaries. For that, we use a region-based force inspired by the unsupervised region-based segmentation model proposed by Chan and Vese [26]. This force is derived from the following energy designed to be minimal when the mean of a region Ω defined in the target image by the evolving level set function (or label function) is close to the mean of the corresponding region in the reference image

$$E = \int_{\Omega_{\text{in}}} |I(x) - \mu_{\text{in}}^{\text{prior}}|^2 dx + \int_{\Omega_{\text{out}}} |I(x) - \mu_{\text{out}}^{\text{prior}}|^2 dx \quad (8)$$

where Ω_{in} is the image area inside the contour and Ω_{out} is the image area outside the contour, μ_{prior} is the prior mean of a given region extracted from a reference image (the atlas) and I is the intensity function of the image to segment. This force assumes that corresponding regions between the reference and the target images have similar means [4]. Note that μ^{prior} does not evolve during the registration process. Hence it is computed once on the reference image in a pre-process step.

Once the dense deformation field matching the atlas to the patient image is computed, the segmentation process ends up as the classical atlas-based method. The transformation is applied to the manually segmented lymph nodes of the atlas image for automatically obtaining the lymph node regions segmentation on the patient's image.

III. Dataset, Preprocessing and Parameters Setting

The dataset used in this paper contains the H&N CT scans of ten patients, acquired during routine clinical practice, at Divisions of Radiotherapy, Geneva University Hospital (HUG). The CT images of the patients in the dataset have significant anatomical variations among them and thereby representing a real time clinical situation. For evaluating the performance of the automated segmentation, the radiation oncologist has manually segmented the lymph nodes for the CT images in the dataset, according to the consensus given in [3]. The size of each slice is 512×512 pixels with a spacing of 0.9375 mm $\times$ 0.9375 mm; the inter-slice distance is 3 mm. A subset of slices that are relevant to the lymph nodes of the H&N region are selected for each patient; this is done by choosing the slices starting from the eye of each patient till the slice that covers the last lymph

[4]Possible intensity differences between both images can be reduced in a pre-process step by histogram matching.

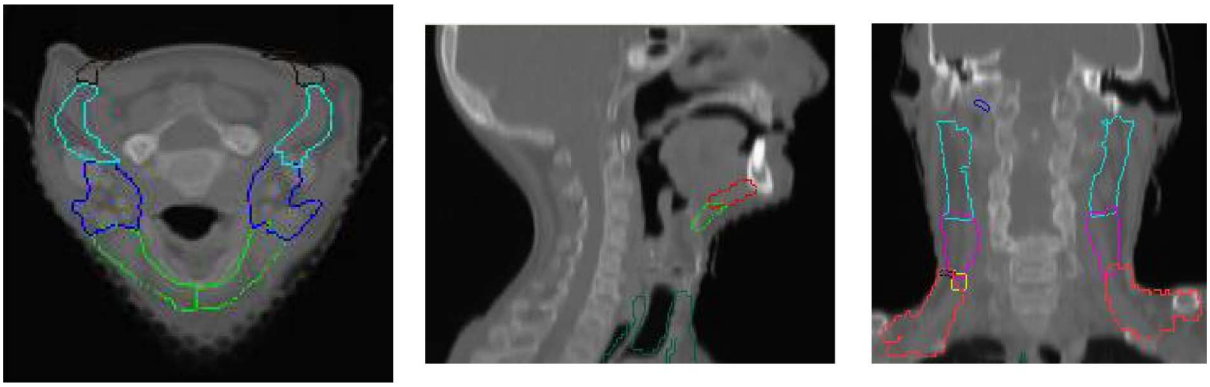

Fig. 6. One of the patients' image in the (I) axial, (II) sagittal, and (III) coronal slices. Automated segmentations of the lymph node regions are superposed over the patient's image.

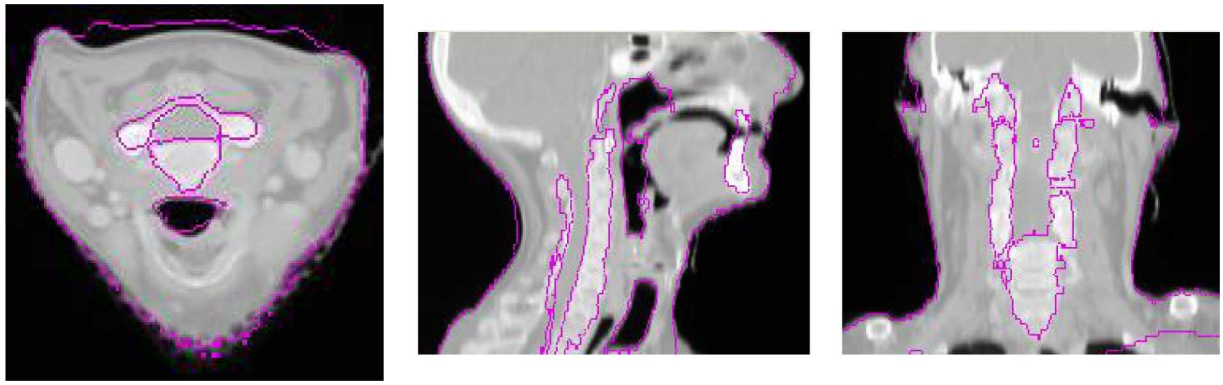

Fig. 7. Contours of structures in the deformed label are superposed over the patient's image, for qualitative evaluation of the registration.

node (lymph node-VI). The images are then preprocessed by thresholding them over a selected region, for removing the bed and other immobilization devices. The CT image shown [5] in Fig. 4 is arbitrarily chosen as the atlas image for the dataset and the automated segmentation is performed on the remaining nine CT images.

It is common with most of the non-rigid image registration methods to perform an affine or rigid registration prior to the final non-rigid registration, in order to recover large deformations. However, our method is found to be robust enough to accurately perform the registration without requiring any such initial registration and is indeed, because of the labeling approach. So we do not use any initial registration and this is one of the advantages of our registration model, whereas we perform an initial affine registration for the other two methods that we use in this paper for comparison.

Concerning the parameters setting, we use four levels of resolutions for the multi-resolution approach and a $\sigma = 1$ for the Gaussian filtering performing the linear diffusion.

IV. Results

In this section, we present the qualitative and quantitative evaluation of the automated segmentation.

[5]All the actual images are cropped and resized while displaying in this paper, in order to show the lymph node regions and other areas of interest with a better resolution.

A. Qualitative Evaluation

We present here the qualitative results for one of the patients' images in the dataset. Fig. 6 shows the CT images of the patients. Figs. 4 and 5 show respectively the intensity image and the labeled image of the atlas. Manually delineated lymph nodes of the atlas image are shown on the intensity image itself in Fig. 4. For a better 3-D visualization of the lymph node volumes, the original atlas image is thresholded to contain only bones, and the lymph node volumes are shown along with the bones in Fig. 8. Now, as mentioned in the previous Section, non-rigid registration is performed and the resulting dense deformation field is computed. The contours of the deformed structures of the labeled image are superposed over the patient's image for qualitative evaluation and are shown in Fig. 7. It can be seen that the algorithm has registered the selected structures well, except over the upper portion of few axial slices. Although the active contour method is actually capable of registering the contours perfectly, the deviation is due to the trade off between the regularization term that smoothens the deformation field and the attraction term.

In the second step, the dense deformation field is applied to the manually delineated lymph nodes of the atlas image to obtain their segmentations on the patient's image. The auto segmented lymph node regions results are superposed over the patient's image and are shown in Fig. 6. Fig. 9 shows 3-D automated segmentations of lymph node volumes on a thresholded

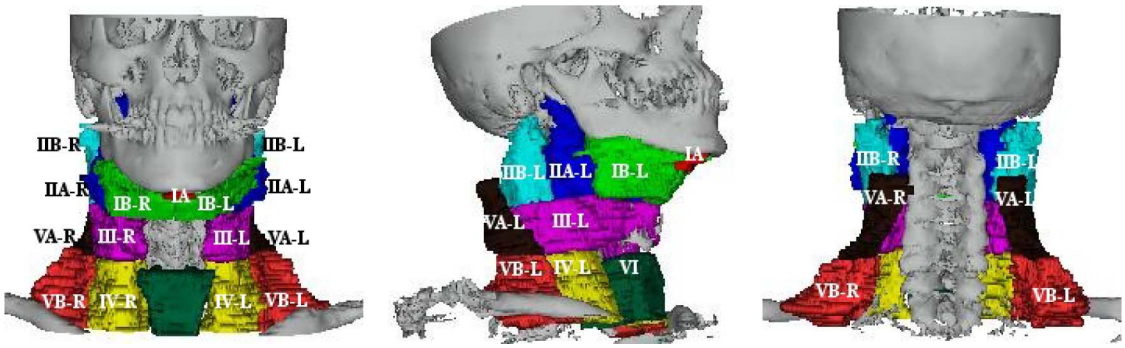

Fig. 8. Manually delineated lymph node volumes on the thresholded atlas image: (I) front view, (II) side view, and (III) back view of the lymph node volumes.

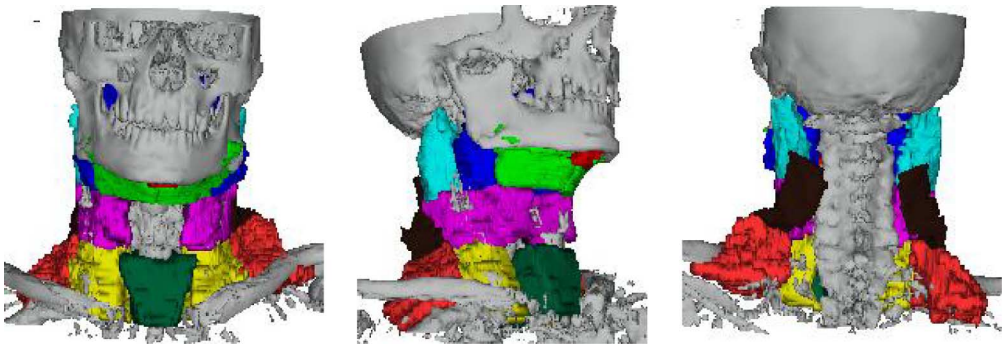

Fig. 9. Automated segmentations of the lymph node volumes on the thresholded patient's image: (I) front view, (II) side view, and (III) back view of the lymph node volumes.

patient's image. These results are visually inspected by an expert oncologist and found to be qualitatively good for most of the lymph nodes.

B. Quantitative Evaluation

The proposed model is compared with the following two registration methods that are commonly used in medical atlas registration.

Radial Basis Function Algorithm (RBF): This is a mutual information-based technique proposed by Rhode *et al.* [16]. The deformation that registers the intensity atlas onto the patient image is modeled with a linear combination of radial basis functions with finite support.

Demons Algorithm: It is an independent implementation of the intensity-based algorithm developed by Thirion [15]. Demons algorithm is close to our method for the following reasons. First, both are non-parametric. Then, both are specially designed to match contours and also both the algorithms use linear diffusion to extend the deformation computed on the contours to the whole image. Finally, both algorithms rely their registration force on polarity. However, in the Demons algorithm, the polarity depends on intensity differences and in our algorithm it depends on the inside and outside of the objects to be registered.

The quantitative evaluation is performed over all the ten CT images in the dataset. The lymph nodes are manually delineated by the radiation oncologist for all the ten patients, and those are considered as the gold standard for evaluating the automated segmentations. The statistics for the left right side pairs of the same lymph node are combined while presenting the results because they are mostly symmetrical. For instance, the statistics for lymph nodes IB-left (IB-L) and IB-right (IB-R) are represented as IB itself. The evaluation is performed using three statistical metrics: sensitivity, specificity, Dice Similarity Coefficient (DSC), and a geometrical metric: Hausdorff distance.

For a lymph node under investigation, an voxel is treated as *True Positive* (TP) if it is present in the lymph node volumes of both the gold standard and the automated segmentation output. Similarly, if an voxel is not present in both gold standard and the automated segmentation, it is treated as a *True Negative* (TN) voxel. If a voxel is present in the gold standard but not in the automated segmentation, it is treated as a *False Negative* (FN) voxel. Finally, if an voxel is present in the automated segmentation but is not in the gold standard, it is treated as a *False Positive* (FP) voxel.

Sensitivity and specificity are the most commonly used statistical metrics and are the measures of "true positive fraction" and "true negative fraction" respectively; they are defined as follows:

$$\text{Sensitivity} = \frac{N_{\text{TP}}}{N_{\text{TP}} + N_{\text{FN}}},$$
$$\text{Specificity} = \frac{N_{\text{TN}}}{N_{\text{TN}} + N_{\text{FP}}}$$

where N_X represents the number of voxels that belong to the category specified by the subscript X. Figs. 10, 11 respectively show the box plots of sensitivity and specificity for each lymph node region, computed from the three methods: RBF algorithm, Demons algorithm and our proposed algorithm. The mean and

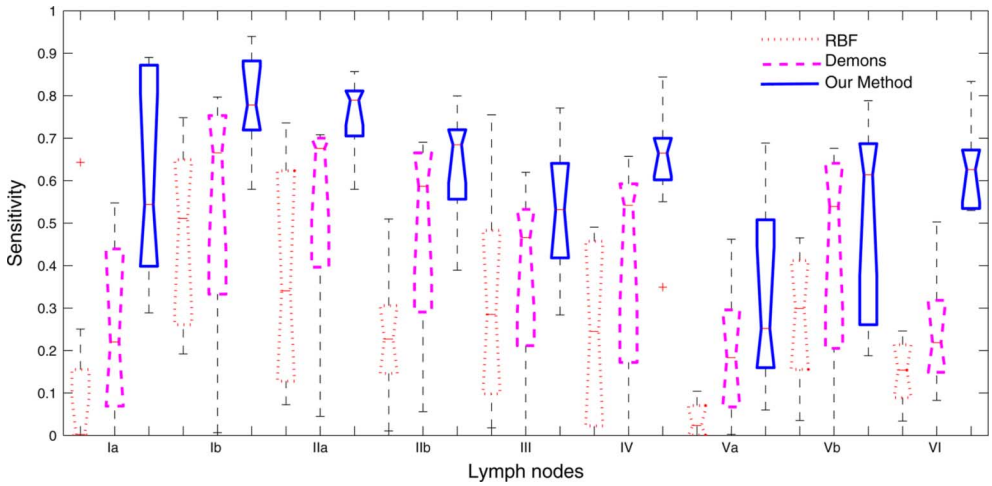

Fig. 10. Box plots comparing the sensitivity measure of lymph node regions segmentation, using (1) RBF algorithm, (2) demons algorithm, and (3) our proposed algorithm.

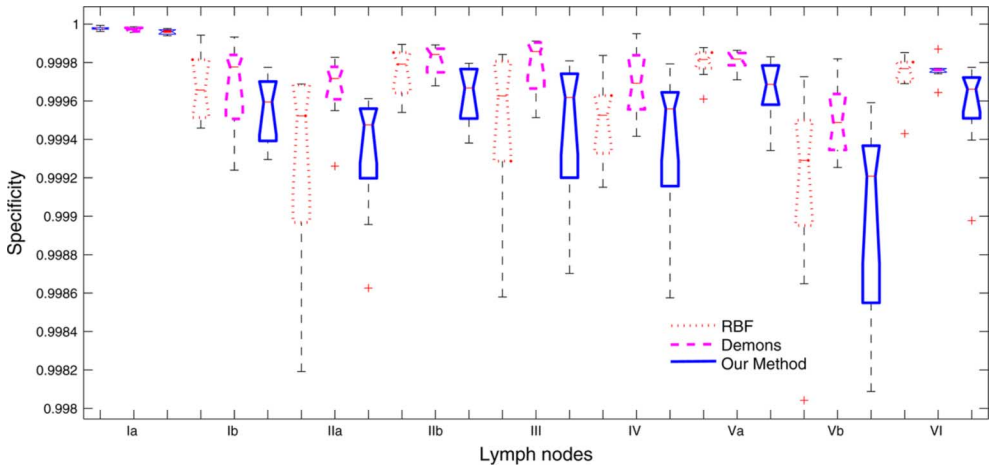

Fig. 11. Box plots comparing the specificity measure of lymph node segmentations, using (1) RBF algorithm, (2) demons algorithm, and (3) our proposed algorithm.

TABLE I
MEAN AND STANDARD DEVIATIONS FOR SENSITIVITY AND DSC MEASURES, ON A DATASET OF TEN PATIENTS

Lymph Node	Sensitivity			DSC		
	RBF	Demons	Our Method	RBF	Demons	Our Method
IA	0.12 ± 0.23	0.25 ± 0.20	0.60 ± 0.25	0.14 ± 0.25	0.22 ± 0.19	0.39 ± 0.14
IB	0.47 ± 0.22	0.54 ± 0.33	0.78 ± 0.12	0.47 ± 0.22	0.50 ± 0.30	0.61 ± 0.06
IIA	0.37 ± 0.27	0.54 ± 0.26	0.76 ± 0.09	0.31 ± 0.18	0.52 ± 0.23	0.58 ± 0.08
IIB	0.24 ± 0.15	0.48 ± 0.26	0.64 ± 0.14	0.27 ± 0.17	0.48 ± 0.24	0.53 ± 0.12
III	0.31 ± 0.26	0.38 ± 0.24	0.53 ± 0.17	0.29 ± 0.20	0.43 ± 0.27	0.48 ± 0.18
IV	0.24 ± 0.22	0.41 ± 0.27	0.64 ± 0.14	0.20 ± 0.22	0.38 ± 0.25	0.41 ± 0.15
VA	0.04 ± 0.04	0.19 ± 0.16	0.32 ± 0.23	0.05 ± 0.05	0.20 ± 0.17	0.27 ± 0.18
VB	0.28 ± 0.16	0.43 ± 0.28	0.51 ± 0.24	0.19 ± 0.16	0.33 ± 0.22	0.31 ± 0.21
VI	0.15 ± 0.08	0.24 ± 0.14	0.63 ± 0.10	0.19 ± 0.11	0.28 ± 0.13	0.53 ± 0.08
Mean	0.25 ± 0.18	0.38 ± 0.24	0.60 ± 0.16	0.23 ± 0.17	0.37 ± 0.22	0.46 ± 0.13

standard deviations for sensitivity are presented in Table I. The results for specificity are not tabulated as the mean values are almost 1 for all methods as we can see in Fig. 11, for the following reason. The major pitfall with specificity is their dependability on the relation between the size of image and object under investigation [14]. Since the sizes of many lymph nodes are small compared to the size of the image, the specificity values in Fig. 11 are close to the ideal value $(=1)$ for all the lymph nodes. Generally, in the axial slice direction of the CT images, the H&N region may not spread over the entire size. Had the CT images been preprocessed in the axial slice direction, by cropping them such that they contain only the H&N region, then for the same automated segmentation results, the specificity values would have decreased. In summary, specificity

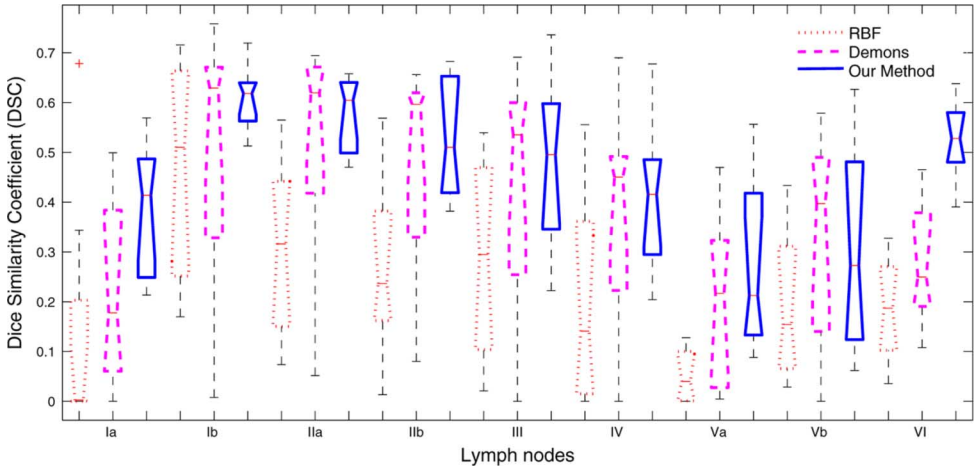

Fig. 12. Box plots comparing the DSC measure of lymph node regions segmentation, using (1) RBF algorithm, (2) demons algorithm, and (3) our proposed algorithm.

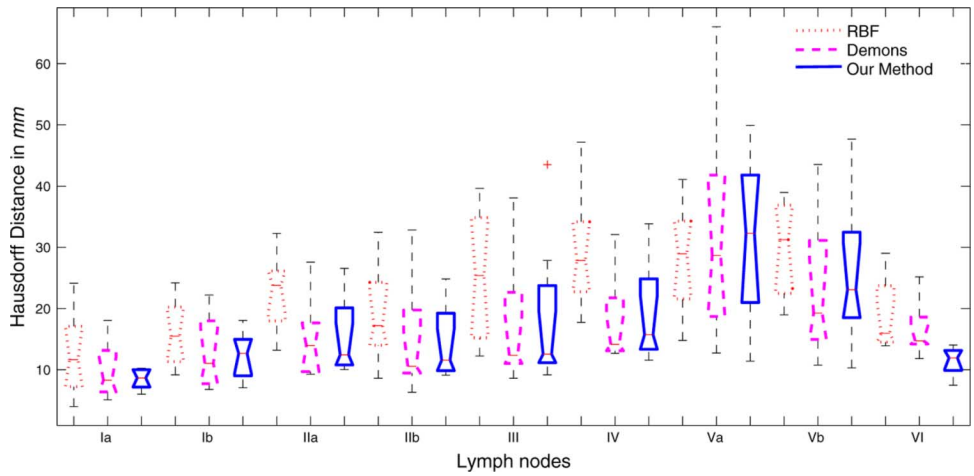

Fig. 13. Box plots comparing the Hausdorff distance measure for lymph node regions segmentation, using (1) RBF algorithm, (2) demons algorithm, and (3) our proposed algorithm.

is not a good measure for evaluating the lymph nodes segmentation, because of its dependance on the relative size of the segmented object with respect to the image size.

DSC is a statistical measure of spatial overlap [27] between the gold standard and the automated segmentation. DSC is defined as follows:[6]

$$\mathrm{DSC} = \frac{2N_{\mathrm{TP}}}{2N_{\mathrm{TP}} + N_{\mathrm{FP}} + N_{\mathrm{FN}}}.$$

The ideal value of DSC is 1. Since DSC does not depend on the size of the samples, it is a more useful measure for quantitative evaluation. Fig. 12 shows the box plots of DSC for each lymph node, computed from all the three methods. The mean and standard deviation values for DSC from the three methods are presented in Table I. The DSC values are good considering the complexity of lymph nodes segmentation but there is still scope for improvement. Since there are no previously reported statistics of DSC for automated segmentation of the H&N lymph node regions, a comparison with the existing techniques is not possible.

[6]Note that the equation that we use here for computing DSC is same as the one used by Warfield *et al.* [27], but just differs in the notation followed.

Hausdorff distance is a measure of resemblance between two sets of data that are superposed on one another [28]. Let the sets $A = \{a_1, \ldots a_m\}$ and $B = \{b_1, \ldots b_n\}$ respectively represent the points of a lymph node in the gold standard and automated segmentations. The Hausdorff distance $H(A, B)$ is defined as

$$H(A, B) = \max(h(A, B), h(B, A))$$

where

$$h(A, B) = \max_{a \in A} \min_{b \in B} ||(a - b)||$$

and $||\cdot||$ is the L_2 norm between the points of A and B. The Hausdorff distance $H(A, B)$ is the maximum of $h(A, B)$ and $h(B, A)$. Thus it measures the degree of mismatch between the gold standard and the automatically segmented lymph node regions, by measuring the distance of the points of gold standard that is farthest from any point of automatically segmented lymph node regions and vice versa. Lesser the Hausdorff distance, better the resemblance between the gold standard and the auto segmentation. Fig. 13 shows the box plots of Hausdorff distance for each lymph node, from all the three methods

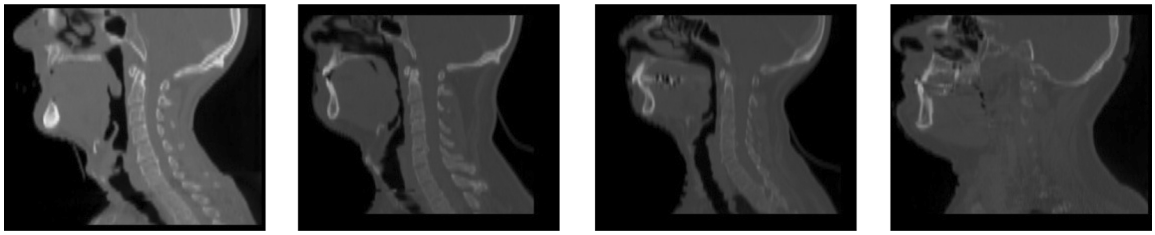

Fig. 14. Sagittal views of four patients in the current dataset. The images illustrate the anatomical variations present in the current dataset.

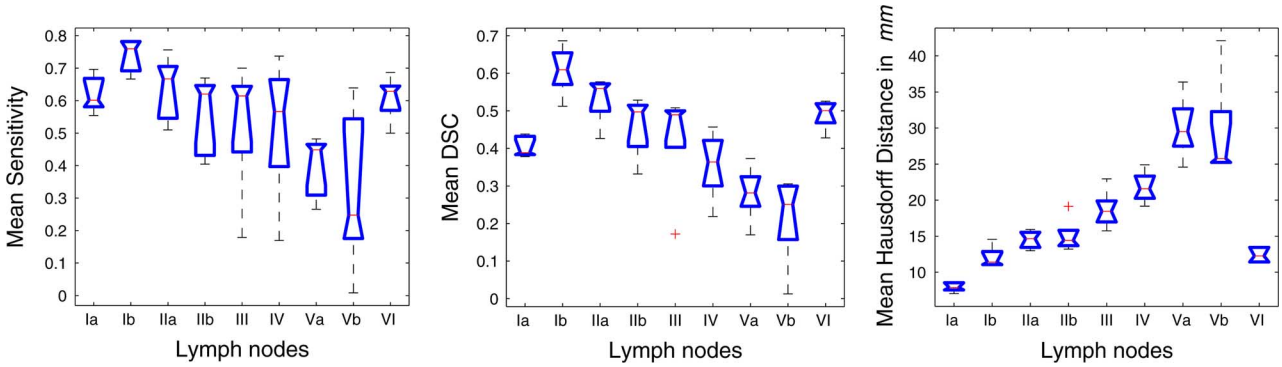

Fig. 15. Box plots of the mean values of sensitivity, DSC, and Hausdorff Distance. These values are computed by varying the atlas through leave-one-out procedure.

TABLE II
MEAN AND STANDARD DEVIATIONS FOR HAUSDORFF DISTANCE MEASURE, ON A DATASET OF TEN PATIENTS

Lymph Node	Hausdorff Distance (mm)		
	RBF	Demons	Our Method
IA	12.51 ± 6.76	9.86 ± 4.53	8.49 ± 1.58
IB	15.93 ± 5.69	12.82 ± 6.17	12.31 ± 3.80
IIA	22.66 ± 6.12	14.93 ± 6.21	15.41 ± 6.74
IIB	19.00 ± 7.67	14.84 ± 9.08	14.41 ± 6.11
III	25.36 ± 10.64	17.34 ± 10.93	18.45 ± 11.85
IV	29.31 ± 9.43	17.84 ± 7.31	19.16 ± 9.10
VA	28.19 ± 8.74	32.14 ± 17.95	31.43 ± 13.49
VB	29.89 ± 7.85	23.12 ± 12.02	25.76 ± 12.31
VI	18.92 ± 6.13	16.51 ± 4.44	11.43 ± 2.27
Mean	22.42 ± 7.67	17.71 ± 8.74	17.43 ± 7.47

and the associated mean and standard deviation are presented in Table II.

Note that there is no *definite relationship* among the trends of the metrics that are considered here for evaluation, because of the following reasons. Sensitivity and DSC are statistical metrics and do not reflect the magnitude of deviations in terms of distance, between the gold standard and the automated segmentation. On the other hand, Hausdorff distance is a geometrical metric that takes these deviations into account, and thus evaluates the segmentation in an entirely different perspective compared to the statistical metrics. Within the two statistical metrics, unlike DSC, sensitivity does not depend on the number of false positive voxels (N_{FP}) thus, no *definite relationship* is possible between the trends of sensitivity and DSC as well.

C. Effect of Atlas Selection

As mentioned earlier, there can be significant anatomical variations in the H&N lymph node regions among different patients. Hence, the evaluation of robustness of a method to the *atlas selection* is particularly important in the current context. We present here the evaluation of robustness of the proposed method, through *"leave-one-out"* atlas selection procedure: One of the images from the dataset of ten patients is chosen as the atlas, and segmentation is performed on the remaining nine patients. The mean values of sensitivity, DSC and Hausdorff distance are computed over the nine patients, for each lymph node region. Then this process is repeated such that each patient in the dataset is used once as the atlas and the segmentation is performed on the remaining nine patients.

Sagittal views of four patients are presented in Fig. 14 for illustrating the anatomical variability present the current dataset. Fig. 15 shows the box plots of mean values of sensitivity, DSC and Hausdorff distance with the varying atlas image. The associated mean and standard deviations of the "mean values of the metrics" are presented in Table III. It can be noticed that final mean values in Table III are very close to the mean values of the metrics in Tables I and II. The standard deviations of the "mean values of the metrics" in Table III are also similar to the standard deviations of the metrics in Tables I and II. Thus the proposed scheme is found to be robust in segmenting the lymph node regions.

V. DISCUSSION AND CONCLUSIONS

In this paper, we have presented the automated segmentation of the H&N lymph node regions, using active contour-based atlas registration technique. We have also proposed to segment the lymph node regions based on the dense deformation field computed from the registration of selected structures that have distinct boundaries. The results from our registration model are compared with the results from RBF algorithm and Demons algorithm, using different statistical and geometrical measures.

TABLE III
MEAN AND STANDARD DEVIATIONS FOR "MEAN VALUES OF THE METRICS," COMPUTED FROM LEAVE-ONE-OUT ATLAS SELECTION PROCEDURE

Lymph Node	Mean Sensitivity	Mean DSC	Mean Hausdorff Distance (mm)
IA	0.62 ± 0.21	0.40 ± 0.13	7.96 ± 1.88
IB	0.74 ± 0.11	0.61 ± 0.06	12.06 ± 2.91
IIA	0.64 ± 0.10	0.53 ± 0.08	14.52 ± 3.70
IIB	0.56 ± 0.14	0.46 ± 0.12	15.06 ± 4.52
III	0.53 ± 0.14	0.43 ± 0.13	18.68 ± 8.62
IV	0.52 ± 0.14	0.36 ± 0.14	21.81 ± 10.41
VA	0.40 ± 0.19	0.28 ± 0.16	30.07 ± 10.25
VB	0.33 ± 0.16	0.21 ± 0.16	29.45 ± 10.43
VI	0.61 ± 0.10	0.49 ± 0.09	12.41 ± 2.95
Mean	0.55 ± 0.14	0.42 ± 0.12	18.00 ± 6.18

Even though multiple structures of the atlas image are used for segmentation, it is not required to perform separate segmentations of these structures because of the labeling strategy. The object-based forces of the active contour model used by our algorithm need the initial positions of the selected structures. These initial positions are given by the labeled image. Then the active contours automatically segment the target objects in the patient's image. The automatic segmentation process is in fact performed by minimizing the energy from which the object-based forces are derived. The only exception where an initial alignment or affine registration is required is, when there is no overlap between the labels of the atlas image and the corresponding structures in the patient's image. This limitation comes from the active contours framework itself. Although there are large deformations among the atlas and the patient's image, as long as there is an overlap of the selected structures, our method is found to perform the registration well without requiring any initial affine registration. All the CT images of the dataset are taken on the same machine having similar orientations. Hence, no initial registration is performed for our method whereas prior affine registration is performed for both RBF and Demons methods.

From the comparison of sensitivity results shown in Fig. 10, our model has performed better than RBF and Demons algorithms. In case of specificity measure, the results for all the lymph node regions, from all the methods are around the ideal value $(=1)$. Specificity is not a good measure for the evaluation of lymph node segmentation, because of it's dependency on the relative size of the lymph node with respect to the image size.

For DSC measure shown in Fig. 12, our method is superior to the RBF method. The reason for lower values of DSC for RBF method is because it is a parametric method and hence cannot cope up with large deformations between the atlas and the patient's image. The mean values of DSC from our method are very close to the Demons method; this is not surprising because both of these techniques are non-parametric, and also both of them are derived from the optical flow model. The variance in DSC is relatively small for our method compared to the Demons method.

As mentioned in the previous Section, lower values of Hausdorff distance imply a better resemblance between the gold standard and the automated segmentation. From the Hausdorff distance results shown in Fig. 13, the results are poor for the RBF method. The mean values of Hausdorff distance for our method are close to the Demons because of the similar reasons mentioned for DSC. For some lymph node regions, the mean values are slightly better for Demons method and is in the other way some other lymph node regions. However, Our method has the advantage of relatively small value of variance than the Demons method.

It can be observed from the results in Tables I and II that for most of the cases, all the three metrics have similar trends; i.e., if the value of one of the metrics is comparatively better for a certain lymph node region, the values of the remaining metrics for that lymph node region are also found to be comparatively better, and vice versa. However, the trends are in the reverse way for few other cases. For instance, using the proposed method, segmentation of lymph node region III has less sensitivity compared to lymph node region IV, but DSC value is comparatively better for lymph node region III. Hence, as mentioned in Section IV-B, there is no *definite relationship* among the trends of these metrics.

The robustness of the method to the atlas selection is also evaluated by selecting each image in the dataset as the atlas, and performing the segmentation of the lymph node regions on the rest of the images in the dataset. The proposed method is found to be robust to the atlas selection. The segmentation results may further improve if *individual atlases* are selected for each patient's image to be segmented, based on the anatomical similarity. but this is beyond the scope of this paper.

In our current evaluation, the manual delineations made by a single radiation oncologist are taken as gold standard. However, there can be some amount of errors in the manual segmentations due to the intra-expert variability, and that needs to be considered. A more accurate performance characterization can be done by obtaining manual segmentations from many experts and then computing a probabilistic estimate of the true segmentation, using the algorithm proposed by Warfield *et al.* in [29].

For computing the dense deformation field in the registration process, we have used four important structures with distinct boundaries: external contour, mandible, vertebrae, and trachea. In the future work, we will include more structures with distinct boundaries to further improve the segmentation results. We also want to extend our evaluation over a larger dataset as the current dataset contains only ten patients.

ACKNOWLEDGMENT

The active contour-based atlas registration model used in this paper was implemented in the ITK [30] environment.

REFERENCES

[1] O. B. Wijers, P. C. Levendag, T. Tan, E. B. Van Dieren, J. Van Sornsen De Koste, H. Van Der Est, S. Senan, and P. J. C. M. Nowak, "A simplified CT-based definition of the lymph node levels in the node negative neck," *Radiother. and Oncol.*, vol. 52, no. 1, pp. 35–42, 1999.

[2] S. Song, W. A. Tome, M. P. Mehta, and P. M. Harari, "Emphasizing conformal avoidance versus target definition for IMRT planning in H&N cancer," *Int. J. Radiation Oncol. Biol. Phys.*, vol. 57, no. 2, pp. S299–S300, Oct. 2003, suppl. 1.

[3] V. Grégoire, P. Levendag, K. K. Ang, J. Bernier, M. Braaksma, V. Budach, C. Chao, E. Coche, J. S. Cooper, G. Cosnard, A. Eisbruch, S. El-Sayed, B. Emami, C. Grau, M. Hamoir, N. Lee, P. Maingon, K. Muller, and H. Reychler, "CT-based delineation of lymph node levels and related CTVs in the node-negative neck: DAHANCA, EORTC, GORTEC, NCIC, RTOG consensus guidelines," *Radiother. and Oncol.*, vol. 69, no. 3, pp. 227–236, 2003.

[4] J. Rogowska, K. Batchelder, G. Gazelle, E. Halpern, W. Connor, and G. Wolf, "Evaluation of selected two-dimensional segmentation techniques for computed tomography quantification of lymph nodes," *Investig. Radiol.*, vol. 13, 1996.

[5] D. M. Honea and W. E. Snyder, , K. M. Hanson, Ed., *Three-Dimensional Active Surface Approach to Lymph Node Segmentation*. Philadelphia, PA: SPIE, 1999, vol. 3661, pp. 1003–1011, 1.

[6] J. Yan, T.-G. Zhuang, B. Zhao, and L. H. Schwartz, "Lymph node segmentation from CT images using fast marching method," *Computeria. Med. Imag. and Graph.*, vol. 28, no. 1–2, pp. 33–38, Jan. 2004.

[7] J. Yan, B. Zhao, L. Wang, A. Zelenetz, and L. H. Schwartz, "Marker-controlled watershed for lymphoma segmentation in sequential CT images," *Med. Phys.*, vol. 33, no. 7, pp. 2452–2460, 2006.

[8] J. Dornheim, H. Seim, B. Preim, I. Hertel, and G. Strauss, "Segmentation of neck lymph nodes in CT datasets with stable 3D mass-spring models: Segmentation of neck lymph nodes," *Academ. Radiol.*, vol. 14, no. 11, pp. 1389–1399, Nov. 2007.

[9] C.-C. Teng, L. G. Shapiro, and I. Kalet, "Head and neck lymph node region delineation using a hybrid image registration method," in *Proc. 3rd IEEE Int. Symp. Biomedical Imaging: From Nano to Macro - Proceedings*, 2006, pp. 462–465.

[10] D. Mattes, D. R. Haynor, H. Vesselle, T. K. Lewellen, and W. Eubank, "PET-CT image registration in the chest using free-form deformations," *IEEE Trans. Med. Imag.*, vol. 22, no. 1, pp. 120–128, 2003.

[11] O. Commowick, V. Grégoire, and G. Malandain, "Atlas-based delineation of lymph node levels in head and neck computed tomography images," *Radiother. Oncol.*, vol. 87, no. 2, pp. 281–289, 2008.

[12] S. Ourselin, A. Roche, S. Prima, and N. Ayache, "Block matching: A general framework to improve robustness of rigid registration of medical images," *Proc. Medical Image Computing and Computer-Assisted Intervention (MICCAI)*, pp. 557–566, 2001.

[13] O. Commowick and G. Malandain, "Evaluation of atlas construction strategies in the context of radiotherapy planning," in *Proc. SA2PM Workshop (From Statistical Atlases to Personalized Models)*, Copenhagen, Denmark, Oct. 2006, held in conjunction with MICCAI 2006.

[14] A. Popovic, M. Engelhardt, and K. Radermacher, "Segmentation of skull-infiltrated tumors using ITK: Methods and validation," *Insight J.*, 2005.

[15] J.-P. Thirion, "Image matching as a diffusion process: An analogy with Maxwell's Demons," *Med. Image Anal.*, vol. 2, no. 3, pp. 243–260, 1998.

[16] G. Rohde, A. Aldroubi, and B. Dawant, "The adaptive bases algorithm for intensity-based nonrigid image registration," *IEEE Trans. Med. Imag.*, vol. 22, no. 11, pp. 1470–1479, Nov. 2003.

[17] B. C. Vemuri, J. Ye, Y. Chen, and C. M. Leonard, "Image registration via level-set motion: Applications to atlas-based segmentation," *Med. Image Anal.*, vol. 7, no. 1, pp. 1–20, 2003.

[18] A. Yezzi, L. Zollei, and T. Kapur, "A variational framework for joint segmentation and registration," in *Proc. IEEE Workshop on Mathematical Methods in Biomedical Image Analysis (CVPR-MMBIA)*, 2001, pp. 44–49.

[19] S. Osher and J. Sethian, "Fronts propagating with curvature-dependent speed—Algorithms based on Hamilton-Jacobi formulations," *J. Comput. Phys.*, vol. 79, no. 1, pp. 12–49, 1988.

[20] J. L. Barron, D. J. Fleet, and S. S. Beauchemin, "Performance of optical flow techniques," *Int. J. Comput. Vis.*, vol. 12, no. 1, pp. 43–77, 1994.

[21] J. Lie, M. Lysaker, and X. Tai, "A binary level set model and some applications to mumford-shah image segmentation," *IEEE Trans. Image Process.*, vol. 15, no. 5, pp. 1171–1181, May 2006.

[22] V. Duay, M. Bach Cuadra, X. Bresson, and J.-P. Thiran, "Dense deformation field estimation for atlas registration using the active contour framework," in *Proc. 14th European Signal Processing Conf. (EUSIPCO)*, Florence, Italy, 2006.

[23] V. Duay, N. Houhou, and J.-P. Thiran, "Atlas-based segmentation of medical image locally constrained by level sets," in *Proc. IEEE Int. Conf. Image Processing (ICIP)*, Genova, Italy, 2005.

[24] V. Duay, X. Bresson, N. Houhou, M. Bach Cuadra, and J.-P. Thiran, "Registration of multiple regions derived from the optical flow model and the active contour framework," in *Proc. 15th European Signal Processing Conf. (EUSIPCO)*, Poznan, Poland, 2007.

[25] V. Duay, "Dense Deformation Field Estimation for Atlas Registration Using the Active Contour Framework" Ph.D. dissertation, Ecole Polytechnique Fédérale de Lausanne, Lausanne, Switzerland, 2007 [Online]. Available: http://library.epfl.ch/theses/?nr=3979

[26] T. F. Chan and L. A. Vese, "Active contours without edges," *IEEE Trans. Image Process.*, vol. 10, no. 2, pp. 266–277, Feb. 2001.

[27] K. H. Zou, S. K. Warfield, A. Bharatha, C. M. C. Tempany, M. R. Kaus, S. J. Haker, W. M. Wells III, F. A. Jolesz, and R. Kikinis, "Statistical validation of image segmentation quality based on a spatial overlap index," *Academic Radiol.*, vol. 11, no. 2, pp. 178–189, 2004.

[28] D. Huttenlocher, D. Klanderman, and A. Rucklige, "Comparing images using the Hausdorff distance," *IEEE Trans. Pattern Anal. Mach. Intell.*, vol. 15, no. 9, pp. 850–863, Sep. 1993.

[29] S. K. Warfield, K. H. Zou, and W. M. Wells, "Simultaneous truth and performance level estimation (STAPLE): An algorithm for the validation of image segmentation," *IEEE Trans. Medical Imag.*, vol. 23, no. 7, pp. 903–921, Jul. 2004.

[30] L. Ibanez, W. Schroeder, L. Ng, and J. Cates, *The ITK Software Guide*, 2nd ed. New York: Kitware, Inc., 2005, ISBN 1-930934-15-7.

Subrahmanyam Gorthi received the Bachelor's degree in electrical and electronics from VRSEC, Vijayawada, India, in 2002 and the Master's degree in computational science from Supercomputer Education and Research Centre (SERC), Indian Institute of Science (IISc), Bangalore, India, in 2006. He is currently pursuing the Ph.D. degree from the Swiss Federal Institute of Technology (EPFL), Lausanne, Switzerland.

He joined the Signal Processing Laboratory (LTS5) of EPFL in 2007. His research interests are medical image registration and segmentation.

Valérie Duay received the M.S. degree in electrical engineering and the Ph.D. degree from the Swiss Federal Institute of Technology (EPFL), Lausanne, Switzerland, in 2002 and 2007, respectively. Her Ph.D. dissertation was related to atlas registration using the active contour framework.

She is currently a Professor in the Institute of Bio-Engineering, University of Applied Sciences Western Switzerland (HES-SO Genéve). Her current scientific interests include atlas-based segmentation, joint registration and segmentation models, and active contours.

Nawal Houhou received the Master's degree in mathematics vision and learning from the Ecole Normale Supérieure, Cachan, France, in 2004. She is currently pursuing the Ph.D. degree at the Swiss Federal Institute of Technology (EPFL), Lausanne, Switzerland.

In November 2004, she joined the Signal Processing Laboratory (LTS5) Group of EPFL. Her current research focuses on medical and natural image segmentation.

Meritxell Bach Cuadra received the telecommunication engineering (ETSETB) degree from the Universitat Politécnica de Catalunya (UPC), Catalunya, Spain, in 1999 and the Ph.D. degree from the Swiss Federal Institute of Technology (EPFL), Lausanne, Switzerland, in 2003 for her work "Atlas-based Segmentation and Classification of Magnetic Resonance Brain Images."

She joined the Computer Vision and Image Analysis Group of the Signal Processing Laboratory (LTS), EPFL, in December 1999. She is currently with the Signal Processing Core of the Biomedical Imaging Center (CIBM), responsible for signal processing research at the Lausanne University Hospital (CHUV). Her main goal is to coordinate the Medical Image Analysis Group research at LTS5 with the needs of expertise in signal/image processing of physicians and researchers at CHUV. Her main research interests are related to magnetic resonance (MR) and diffusion MR imaging, atlases, registration, segmentation, and classification.

Ulrike Schick graduated in medicine from the Johannes Gutenberg University, Mainz, Germany, in 2005.

She then joined Geneva University Hospital (HUG), Geneva, Switzerland, for a special training in radiation oncology. She is mainly interested in the study and treatment of head and neck cancer and brain tumors.

Minerva Becker studied medicine at the University of Berne, Berne, Switzerland and specialized in radiology at the Insel Hospital, Berne.

She is currently in charge of the Imaging Unit of Head and Neck and Maxillofacial Radiology at the Geneva University Hospital, Geneva, Switzerland. Previously, she was with the Armed Forces Institute of Pathology (AFIP), Washington, DC, as well as Duke University, Durham, NC, where she was involved in clinical research projects. She specialized early in her career in the field of head and neck radiology and many of her scientific publications focus on radiologic-pathologic correlation issues, as well as on the performance of MRI and CT in assessing head and neck tumors. She is the author of over 75 publications in the field of head and neck radiology and is co-editor of *Head and Neck Imaging* (Philadelphia, PA: WB Saunders, 2004). Her main fields of interest include head and neck oncology, larynx, salivary glands and base of the skull, new imaging developments and teaching young residents, as well as training fellows specialized in the field of head and neck radiology.

Abdelkarim S. Allal is Senior Lecturer at the Geneva Medical School, Geneva, Switzerland, and Chairman of the Radiation Oncology Division at the HFR—Fribourg Hospital, Fribourg, German. He is author or co-author of more than 90 papers in peer-review journals, four book chapters, and more than 100 abstracts of international or national meetings. He is President of the Swiss Head and Neck Cancer Collaborative Group and a member of six international and national scientific societies.

Jean-Philippe Thiran (M'93–SM'05) was born in Namur, Belgium, in 1970. He received the Elect. Eng. and Ph.D. degrees from the Universite Catholique de Louvain (UCL), Louvain-la-Neuve, Belgium, in 1993 and 1997, respectively.

He joined the Signal Processing Institute (ITS), Swiss Federal Institute of Technology (EPFL), Lausanne, Switzerland, in February 1998 as a Senior Lecturer. Since January 2004, he has been an Assistant Professor, responsible for the Image Analysis Group. His current scientific interests include image segmentation, prior knowledge integration in image analysis, partial differential equations and variational methods in image analysis, multimodal signal processing, medical image analysis, including multimodal image registration, segmentation, computer-assisted surgery, and diffusion MRI. He is author or co-author of six book chapters, 65 journal papers, and some 115 peer-reviewed papers published in proceedings of international conferences. He holds four international patents.

Dr. Thiran was Co-Editor-in-Chief of *Signal Processing* from 2001 to 2005. He is currently an Associate Editor of the *International Journal of Image and Video Processing* and a member of the Editorial Board for *Signal, Image and Video Processing* (published by Springer). He was the General Chairman of the 2008 European Signal Processing Conference (EUSIPCO 2008).